ACS APPLIED MATERIALS & INTERFACES

www.acsami.org

Research Article

Patterning Graphene Films by H_2O-Based Magnetic-Assisted UV Photolysis

Shubin Su, Hao Li, Jingxian Huang, Zhibin Zhang, Chenhui Liang, Wenxiang Jiang, Aolin Deng, Kaihui Liu, Zhiwen Shi, Dong Qian, and Haihua Tao*

Cite This: *ACS Appl. Mater. Interfaces* 2020, 12, 55382−55389

Read Online

ACCESS | Metrics & More | Article Recommendations | Supporting Information

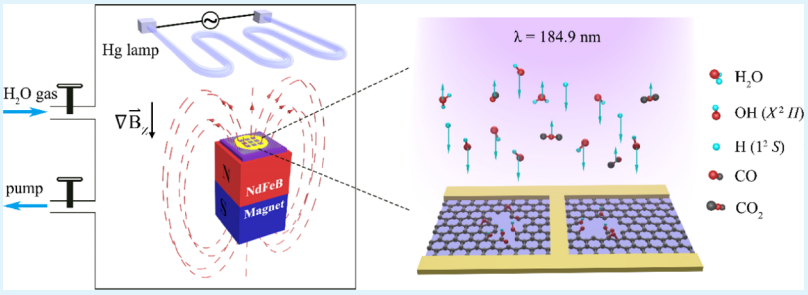

ABSTRACT: Properly cutting graphene into certain high-quality micro-/nanoscale structures in a cost-effective way has a critical role. Here, we report a novel approach to pattern graphene films by H_2O-based magnetic-assisted ultraviolet (UV) photolysis under irradiation at 184.9 nm. By virtue of the paramagnetic characteristic, the photo-dissociated hydroxyl [$OH(X^2\Pi)$] radicals are magnetized and have their oxidation capability highly enhanced through converting into an accelerated directional motion. Meanwhile, the precursor of $H_2O(\tilde{X}^1A_1)$ molecules distributes uniformly thanks to its weak diamagnetic characteristic, and there exists no instable diamagnetic intermediate to cause lateral oxidation. Possessing these unique traits, the H_2O-based magnetic-assisted UV photolysis has the capability of making graphene microscale patterns with the linewidth down to 8.5 μm under a copper grid shadow mask. Furthermore, it is feasible to pattern graphene films into 40 nm-wide ribbons under ZnO nanowires and realize hybrid graphene/ZnO nanoribbon field-effect transistors with a hole mobility up to 7200 $cm^2 \cdot V^{-1} \cdot s^{-1}$. The X-ray photoelectron spectroscopy and time-of-flight secondary ion mass spectrometry analyses reveal that $OH(X^2\Pi)$ radicals act as a strong oxidant and that another product of $H(1^2S)$ adsorbs weakly on graphene.

KEYWORDS: *chemical vapor deposition, H2O-based magnetic-assisted UV photolysis, graphene films, mass spectrometry, high-quality micro-/nanoscale structures*

INTRODUCTION

In addition to the breakthrough of growing large-area high-quality monolayer and multilayer graphene films by chemical vapor deposition (CVD), it is crucial to precisely cut them into certain micro-/nanoscale patterns in order to propel their fundamental studies and versatile applications.[1−5] Nowadays, conventional photolithography and electron-beam lithography, combined with reactive ion etching (RIE), have remained the mainstream techniques, even though they are costly and inevitably incur resist contamination for atomic-layer-thick two-dimensional material.[5−7] To surmount these shortcomings, Yong *et al.* attempted to use hard shadow masks as a substitute for lithography to pattern graphene films by oxygen plasma RIE procedure. However, such obtained graphene pattern had its quality degraded due to severe lateral oxidation.[8] Direct laser writing, another frequently used approach in the semiconductor industry, has been attempted to pattern graphene films despite its prominent problems such as low precision, debris contamination, and substrate damage.[9] Ever since the discovery of graphene, it has always been underway to seek feasible approaches to realize high-quality graphene patterning in an efficient and economical way.[10−16]

Using oxygen molecules [$O_2(X^3\Sigma_g^-)$] as the precursor, magnetic-assisted ultraviolet (UV) ozonation was proposed and tested to be feasible for patterning graphene microstructures under a shadow mask upon irradiation of a xenon excimer lamp (λ = 172 nm).[14] In this novel etching approach, the photo-dissociated paramagnetic oxygen radicals [$O(^3P)$], moving directionally in the inhomogeneous vertical magnetic field after magnetization, play a critical role in the highly enhanced

Received: September 5, 2020
Accepted: November 9, 2020
Published: November 23, 2020

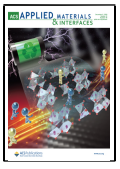

https://dx.doi.org/10.1021/acsami.0c16005
ACS Appl. Mater. Interfaces 2020, 12, 55382−55389

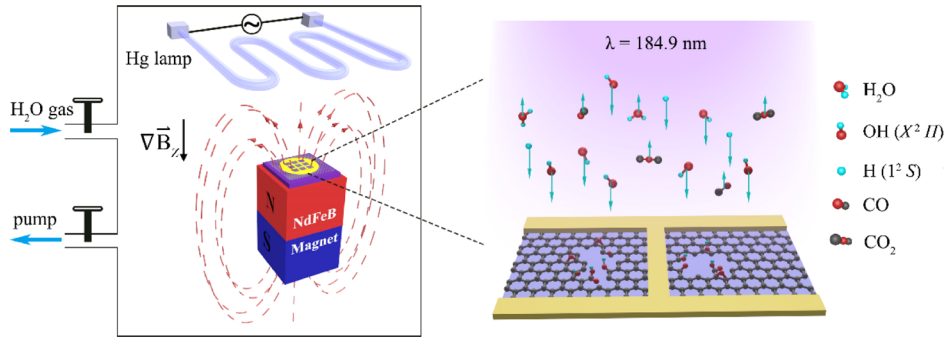

Figure 1. Schematic configuration of H_2O-based magnetic-assisted UV photolysis (left) and its dynamic photochemical reaction focusing on graphene surface (right). Cyan arrows in the right panel represent the magnetic force exerted on the paramagnetic radicals [$H(1^2S)$ and $OH(X^2\Pi)$] and weak diamagnetic substances (H_2O, CO, and CO_2).

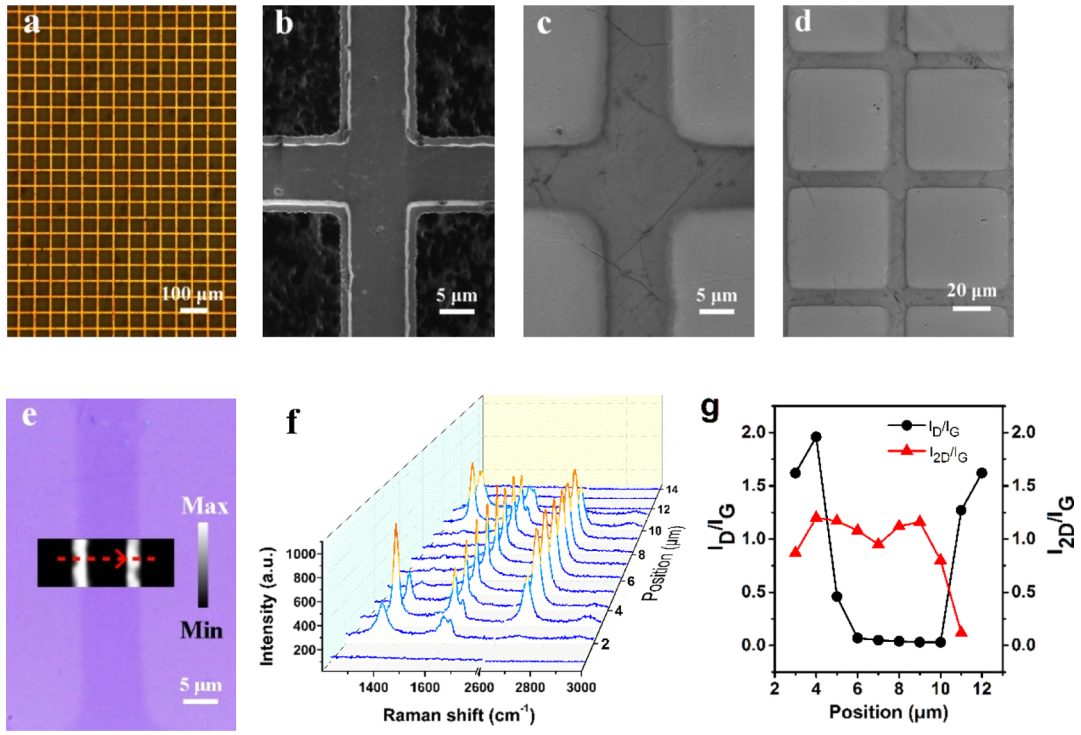

Figure 2. Patterning graphene film through the copper grid shadow mask by H_2O-based magnetic-assisted UV photolysis. (a) Optical image and (b) SEM micrograph image of the mask. (c) SEM topographic image of the patterned graphene microstructure and (d) its zoom-out image. (e) Micro-Raman map of the intensity distribution of D mode across a rib, (f) corresponding Raman spectral evolution along the red dashed arrow line in (e), and (g) I_D/I_G and I_{2D}/I_G as a function of position in (f).

oxidation capability. As a contrast, the main product of oxygen radicals produced in the conventional oxygen plasma RIE process moves randomly in an applied electric bias due to its electrically neutral characteristic and thus induces severe lateral oxidation.[16−18]

The magnetic-assisted UV ozonation, however, has two major drawbacks that restrict the minimum linewidth and its practical applications. First, it appears tricky to precisely control the concentration of $O(^3P)$ radicals since the paramagnetic $O_2(X^3\Sigma_g^-)$ molecules incline to gather around the magnetic poles instead of distributing uniformly in the reaction chamber. Second, the photo-synthesized unstable intermediate of ozone diffuses arbitrarily and therefore can impair the quality of graphene patterning by lateral oxidation.[14,15]

Water [$H_2O(\tilde{X}^1A_1)$], attractive for its potential application in the synthetic chemical fuel production of hydrogen,[19,20] can surmount these obstacles and bring out marvelous opportunities when combined with the UV irradiation and magnetic field thanks to the following three traits. First, $H_2O(\tilde{X}^1A_1)$ molecules, a weak diamagnetic substance, distribute uniformly in the circumstance of an inhomogeneous magnetic field. Second, under the vacuum UV irradiations, $H_2O(\tilde{X}^1A_1)$ molecules photo-dissociate into paramagnetic hydrogen [$H(1^2S)$] and hydroxyl [$OH(X^2\Pi)$] radicals without any intermediate product that can arouse lateral oxidation.[21−25] Third, the paramagnetic $OH(X^2\Pi)$ radicals have a highly enhanced oxidation capability compared with $O(^3P)$ and can enhance the etching efficiency in principle.[10,26]

In this work, we report on the patterning of a graphene film by H_2O-based magnetic-assisted UV photolysis under irradiation at 184.9 nm. In an inhomogeneous vertical magnetic field, the photo-dissociated paramagnetic $OH(X^2\Pi)$ radicals are magnetized and then have an accelerated directional motion toward graphene.[15,19−23] As a consequence, the directional-motion-

https://dx.doi.org/10.1021/acsami.0c16005
ACS Appl. Mater. Interfaces 2020, 12, 55382−55389

induced oxidation enhancement makes it feasible to realize high-resolution micro-/nanoscale graphene patterning.[27−29] The etching mechanism of graphene by H_2O-based magnetic-assisted UV photolysis is explored through X-ray photoelectron spectroscopy (XPS) and time-of-flight secondary ion mass spectrometry (TOF-SIMS) measurements.

RESULTS AND DISCUSSION

Figure 1 shows the schematic configuration of H_2O-based magnetic-assisted UV photolysis designed for patterning graphene films, using a home-designed vacuum machine equipped with a low-pressure mercury (Hg) lamp (λ = 184.9 nm, P = 200 W).[15] The deionized water contained in a self-designed stainless-steel bottle provides gaseous H_2O molecules when connected to the evacuated photochemical reaction chamber. A cuboid-shaped neodymium−iron−boron (NdFeB) permanent magnet put underneath the sample is used to provide the inhomogeneous vertical magnetic field (B_z = 0.57 T, ∇B_z = 160 T·m^{-1}).[14,15]

The H_2O-based magnetic-assisted UV photolysis proceeds as illustrated in the right part of its zoom-in view (Figure 1). The ground-state $H_2O(\tilde{X}^1A_1)$ molecules are excited to the first excited electronic state of $H_2O(\tilde{A}^1B_1)$ upon UV irradiation and then dissociate primarily into paramagnetic $H(1^2S)$ and $OH(X^2\Pi)$ radicals on a time scale of femtosecond as described in eq 1.[21−25,30,31]

$$H_2O(\tilde{X}^1A_1) + h\nu(120 < \lambda \leq 186.4\ \text{nm}) \rightarrow H_2O(\tilde{A}^1B_1) \rightarrow H(1^2S) + OH(X^2\Pi) \quad (1)$$

The available energy in this direct photodissociation is mainly converted into the translational motion of $H(1^2S)$ and $OH(X^2\Pi)$ radicals.[25] In the presence of the inhomogeneous vertical magnetic field, the paramagnetic $H(1^2S)$ and $OH(X^2\Pi)$ radicals are both magnetized and then accelerate toward graphene surface with the magnetic force denoted by cyan arrows in the right part of Figure 1. Specifically speaking, each of the two kinds of radicals has an attractive magnetic force F_z on the order of 10^{-22} N according to the formula $F_z = g_J \cdot \mu_{eff} \cdot \nabla B_z$. Herein, the Landé g_J-factor takes the value of 2 and 4/3 for $H(1^2S)$ and $OH(X^2\Pi)$, respectively;[31] the effective magnetic moment μ_{eff} of $H(1^2S)$ and $OH(X^2\Pi)$ equals to 1 μ_B (μ_B is the Bohr magneton) and 2 μ_B, respectively.[28,32]

The H_2O-based magnetic-assisted UV photolysis can be used to pattern graphene films into high-quality microscale structures with the aid of a copper shadow mask. As shown in Figure 2a, the mask is composed of orthogonal ribs with a period of 62 μm. The high-resolution scanning electron microscopy (SEM) image in Figure 2b (biased at 5 kV) shows that the ribs have a step structure. In detail, the central flat region is ∼7.8 μm wide and ∼6.6 μm thick, and each edge has a width ranging from 1.3 to 1.8 μm with a thickness of ∼3.8 μm. When treated by H_2O-based magnetic-assisted UV photolysis (working distance, *i.e.*, distance between the lamp and graphene: 32 mm; duration: 8 min × 3 times), the polycrystalline graphene can be patterned into 8.5 μm-wide grid microstructures (Figure 2c,d). The pattern has a profile conformal to the shadow mask but with its linewidth falling between the central and total width of the bar. Besides, some filamentary residues exist in the blank area around the graphene edges due to the presence of ripples (see the Supporting Information, Figure S1).

The quality of graphene patterns is further characterized by its lateral oxidation using micro-Raman spectroscopy.[14] Figure 2e shows the defect (D) mode image scanned across a rectangular area which, for clarity, is superimposed on the same position of its optical image. The bright lines distributed along two edges certify lateral oxidation underneath the mask. The Raman spectral evolution scanned along the dashed arrow line across the bar is plotted in Figure 2f. The peak intensity ratios of D to G mode (I_D/I_G) and 2D to G mode(I_{2D}/I_G) are plotted in Figure 2g. Compared with the pristine polycrystalline graphene (see the Supporting Information, Figure S1), we can conclude from Raman characterization that lateral oxidation occurs mainly within 2−3 μm with strong D peaks and that the central region appears slightly oxidized or mechanically damaged by the mask with a decreasing intensity ratio of I_{2D}/I_G compared with pristine graphene (Figure S1). We think this degradation along edges mainly stems from the imperfect vertical magnetic field and the step structure of the mask, that is, its imperfect contact with graphene and the resultant gas diffusion and dissipation in the gap.[14] As elaborately stated in the Supporting Information (Figure S2), the specific shadow mask can impose a great impact on the quality of graphene patterns.

The potential of patterning graphene film by H_2O-based magnetic-assisted UV photolysis is explored by fabricating graphene nanostructures. Figure 3a shows the SEM topographic image of ZnO nanowires distributed irregularly on the high-quality single-crystal CVD grown graphene film. Using the single ZnO nanowire mask (a diameter of ∼75 nm) as outlined by the red dashed rectangle, we can obtain a graphene nanoribbon with a linewidth of ∼40 nm (Figure 3b).

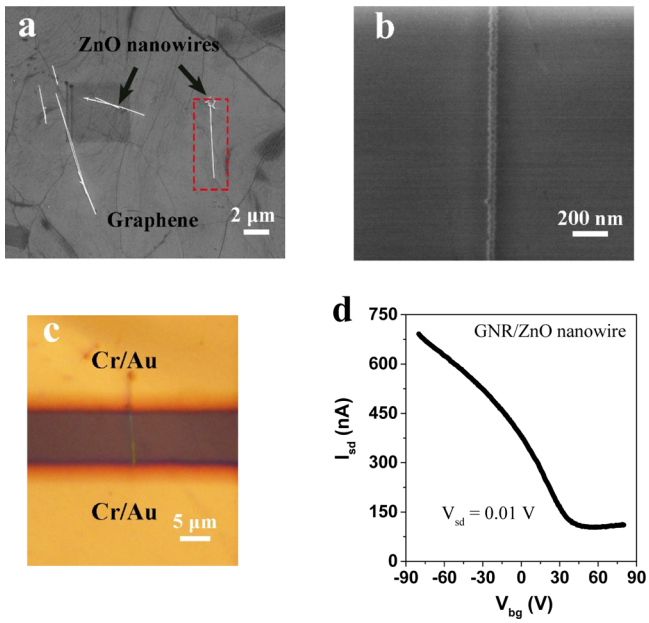

Figure 3. Characterization of graphene nanoribbons patterned under ZnO nanowire mask by H_2O-based magnetic-assisted UV photolysis. (a) SEM image of ZnO nanowires distributed on graphene film. (b) High-resolution SEM image of a pure graphene nanoribbon attained from that covered by ZnO nanowire outlined in (a). (c) Optical image of a hybrid graphene/ZnO nanoribbon FET device, and (d) its drain−source current as a function of back-gate voltage measured in N_2 atmosphere.

The quality of graphene nanoribbons is further characterized by electrical transport measurement. Figure 3c shows the optical image of a hybrid graphene/ZnO nanowire field-effect transistor (FET). In order to avoid any damage to the underneath

https://dx.doi.org/10.1021/acsami.0c16005
ACS Appl. Mater. Interfaces 2020, 12, 55382−55389

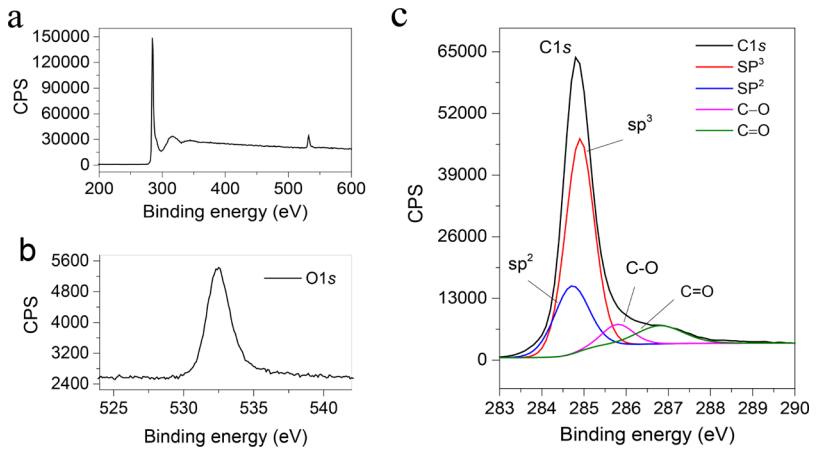

Figure 4. XPS spectra of graphite treated by H_2O-based magnetic-assisted UV photolysis. (a) XPS survey spectrum, (b) highly resolved narrow-band O 1s spectrum, and (c) C 1s spectrum fitted with four mixed Gaussian−Lorentzian curves. CPS stands for counts per second.

graphene nanoribbon, the ZnO nanowire (with a diameter of ∼115 nm) is kept *in situ* throughout the electrical transport measurement with the curve plotted in Figure 3d. The entire graphene nanoribbon (length: ∼8 μm; width estimated from statistics: ∼80 nm) is calculated to have an average hole mobility μ_h of ∼7200 $cm^2 \cdot V^{-1} \cdot s^{-1}$ from the formula $\mu_h = \frac{1}{C_g}\left|\frac{\Delta\sigma}{\Delta V_g}\right|$, where $C_g = 1.15 \times 10^{-8}$ $F \cdot cm^{-2}$ is the gate capacitance, and $\Delta\sigma/\Delta V_g$ is the slope of the conductivity σ varying with the gate voltage V_g near the Dirac point.[6] The good hole mobility obtained at room temperature indicates that the graphene nanowire has a high quality.[3] However, the graphene nanoribbon has a rather poor electron mobility of ∼330 $cm^2 \cdot V^{-1} \cdot s^{-1}$ as calculated from the relatively flat part close to the Dirac point at ∼50 V. This reduction is mainly related to the electron scattering due to the adsorption of chemical functional groups. Herein, we neglect the impact of the remaining mask on the electrical conductivity of graphene since the ZnO nanowire mask has high resistivity (see the Supporting Information, Figure S3). In the highly oxidative environment, the instability of the ZnO nanowire mask (Figure S4) and its passivation (Figure S5) are discussed in the Supporting Information.

The working mechanism of how graphene interacts with the highly accelerated $H(1^2S)/OH(X^2\Pi)$ radicals can be deduced from its varying status of surface chemical functional groups.[14] For this purpose, a piece of graphite treated the same by H_2O-based magnetic-assisted UV photolysis is used for XPS measurement. Compared with the pristine graphite (ref 14), a new peak of O 1s emerges along with the intrinsic C 1s in the survey spectrum (Figure 4a). The O 1s peak situates at 532.5 eV with a full width at half maximum of 1.87 eV as shown in the highly resolved XPS spectrum (Figure 4b). The concentration of atomic oxygen in the treated graphite (within a depth of ∼10 nm) is ∼3.32%, verifying the strong photochemical oxidation from $OH(X^2\Pi)$ radicals.

The exact combination of $OH(X^2\Pi)$ radicals with graphene can be derived from the highly resolved XPS spectrum of C 1s for the photochemically oxidized graphite. As shown in Figure 4c, the spectrum can be fitted with four individual Gaussian−Lorentzian curves each representing a certain chemical functional group. A morphological transition from sp^2 crystalline to sp^3 amorphous structure occurs in the oxidized graphite. At the same time, the C═O and C−O chemical functional groups are introduced in the H_2O-based magnetic-assisted UV photolysis. Herein, the intensity of C═O group appears slightly stronger than that of C−O group, suggesting an oxidation process different from $O(^3P)$ radicals.[14]

It was reported that hydrogen atoms incline to form dimers on graphene through weak physical adsorption and migration[33,34] or chemically bond with graphene to form graphane,[35] or even pattern graphene by anisotropic etching at a high temperature.[36] The exact role of photo-dissociated $H(1^2S)$ radicals in graphene patterning can be tracked by TOF-SIMS measurement of pristine graphite and that treated by H_2O-based magnetic-assisted UV photolysis.[37−39] In order to exclude influence from the atmospheric hydrogen, deuteroxide (D_2O) instead of H_2O was used as the precursor in the magnetic-assisted UV photolysis. In this case, the gaseous $D_2O(\tilde{X}^1A_1)$ molecules photo-dissociate into $D(1^2S)$ and $OD(X^2\Pi)$ radicals under irradiation at 184.9 nm as described in eq 2.[40,41]

$$D_2O(\tilde{X}^1A_1) + h\nu(120 < \lambda \leq 186.4\ \text{nm}) \rightarrow D_2O(\tilde{A}^1B_1) \rightarrow D(1^2S) + OD(X^2\Pi) \quad (2)$$

The isotopic $D(1^2S)$ radicals, which are paramagnetic and supposed to play the same role as $H(1^2S)$ in the photochemical reaction, can be easily discerned when combined with graphene. Meanwhile, the paramagnetic $OD(X^2\Pi)$ radicals act as a strong oxidant resembling $OH(X^2\Pi)$ as confirmed in the Supporting Information (Figure S6).

Figure 5 compares the C_n^--ion (n = 1, 2, 3, 4) calibrated negative mode spectra of pristine graphite and that treated by D_2O-based magnetic-assisted UV photolysis. As observed, the secondary H^-, H_2^-, C_n^-, D^-, and OD^- ions exist in both cases. The H/D-related ion signals in Figure 5a of pristine graphite may be introduced in the growth stage and/or through hydrocarbon adsorption in the post-treatment. For the etched graphite (Figure 5b), the ratio of D^- to H^- ions increases from 1/10,376 (close to that of 1/10,000 in nature) to 1/2208. From another perspective, the intensity of D^- ions increases about 11 times, further verifying the introduction of deuterium atoms to graphite in the photochemical reaction. Since neither C_xD^- nor D_2^- can be detected, deuterium atoms are supposed to bond weakly with graphite rather than in the form of carbon-based materials or D_2O/D_2 molecules.

The OD^- ions, existing in pristine graphite, increase about 28 times after treatment by D_2O-based magnetic-assisted UV photolysis, much higher than the D^- ions. This result reveals that

https://dx.doi.org/10.1021/acsami.0c16005
ACS Appl. Mater. Interfaces 2020, 12, 55382−55389

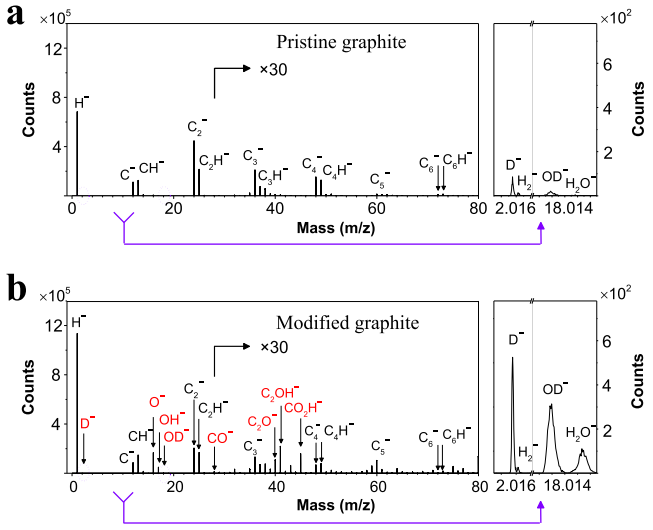

Figure 5. Comparison of TOF-SIMS spectra for pristine graphite and that treated by D_2O-based magnetic-assisted UV photolysis. TOF-SIMS negative ion spectra of (a) pristine graphite and (b) the etched graphite; the two right parts each represent the corresponding zoom-in spectrum focusing on ions with the mass located at around 2 and 18. The intensities in both spectra are multiplied by 30 for ions with the mass exceeding 28.

the number of $OD(X^2\Pi)$ radicals participating in graphite etching far exceed that of the $D(1^2S)$ radicals. Besides, there emerge some other oxygen-containing ions including O^-, CO^-, C_2O^-, OH^-, C_2OH^-, and CO_2H^- in the treated graphite. The comparison confirms oxidation from $OD(X^2\Pi)$ radicals, as well as from $OH(X^2\Pi)$ radicals dissociated from H_2O or some organic molecules inevitably adsorbed in the photochemical reaction chamber.

From the above discussion, we can draw a conclusion that the photo-dissociated $H(1^2S)$ radicals physically adsorb on graphene and that $OH(X^2\Pi)$ radicals act as a strong etchant of graphite as described in eqs 3 and 4.[42]

$$C + OH(X^2\Pi) \rightarrow H_2O(X^1A_1) + CO + CO_2 \quad (3)$$

$$C + OH(X^2\Pi) \rightarrow H_2 + CO + CO_2 \quad (4)$$

The four products of H_2O, H_2, CO, and CO_2 are all diamagnetic with their molar magnetic susceptibilities individually listed in Table 1. From the perspective of graphene, the weak repulsive magnetic forces exerted on these molecules away from its surface can facilitate the ongoing photochemical oxidation.

Table 1. Molar Magnetic Susceptibility of the Gas Products at Room Temperature[26]

gas	H_2O	CO	CO_2	H_2
molar magnetic susceptibility (χ_m: 10^{-6} cm^3·mol^{-1})	−13.1	−9.8	−21.0	−3.99

We have fabricated more than 10 samples of micro/nano FET devices each on the high-quality single-crystal graphene. Although all FET devices are electrically p-type doped, the hole mobility takes values in a wide range determined mainly by the quality of the specific region of transferred graphene. The randomly distributed ripples, local defects, and cracks in graphene have great impact on the electrical property of FET devices. The quality of nanoribbons fluctuates drastically as it is affected by the quality of the exact nanoscale graphene. For microscale graphene FET device, it is unavoidably affected by the ripples. As a consequence, the selected best graphene/ZnO nanoribbon FET device in Figure 3 has a hole mobility far exceeding that of the best microscale one (Figure S2).

It is notable that the inhomogeneous vertical magnetic field is a prerequisite for patterning graphene films by H_2O-based magnetic-assisted UV photolysis. When no magnetic field is supplied, graphene keeps almost intact even though the other photochemical parameters used are the same (see the Supporting Information, Figure S7). This phenomenon reveals that the etching capability of randomly moving $OH(X^2\Pi)$ radicals is drastically reduced compared with the accelerated directional ones.

Using the same shadow masks in Figures 2 and S2, we have patterned graphene microstructures and FET devices by the conventional oxygen plasma RIE technique. The graphene patterns are severely damaged due to lateral oxidation of randomly moving oxygen radicals (see the Supporting Information, Figure S8). When no bias is applied to control the directionality of positive ions in an oxygen plasma machine, graphene pattern cannot form due to the random motion of all reactant molecules, including oxygen radicals and oxygen ions O_2^- (see the Supporting Information, Figure S9). Compared with the conventional oxygen plasma RIE, the H_2O-based magnetic-assisted UV photolysis manifests an outstanding directional etching trait. Furthermore, H_2O-based magnetic-assisted UV photolysis, a combination of the vacuum UV discharge lamp and permanent magnet with H_2O molecules as the oxidant precursor, manifests to be more cost-effective compared with oxygen plasma RIE etching technique for its future industrial applications.

As clarified, the low-pressure mercury lamp instead of the xenon excimer lamp is used as the UV source to pattern graphene micro-/nanoscale structures in the H_2O-based magnetic-assisted UV photolysis. The experimental results indicate that graphene patterns fabricated under UV irradiation of the xenon excimer lamp are inferior in quality due to the limitation of the previous technique (see the Supporting Information, Figure S10).[14] Inspiringly, we have recently circumvented this limitation and realized high-quality graphene patterns with the etching efficiency improved by a few orders. This topic will be discussed in detail elsewhere.

Different shadow masks have been used to pattern graphene films in this work. Although convenient and well demonstrating the etching directionality of H_2O-based magnetic-assisted UV photolysis, the strategy exhibits some limitations as follows. First, shadow masks may damage graphene from the mechanical pressing and scratching due to their direct contact. Second, not all shapes (*e.g.*, a ring) and complex circuit diagrams can be transferred onto a shadow mask. In this case, multiple shadow masks should be carefully designed to avoid freestanding parts and aligned with each other to realize graphene patterns by multiple etching. Third, fabrication of shadow masks with the linewidth down to 10 μm appears difficult. To eliminate these limitations, it is significant to explore the feasibility of combining H_2O-based magnetic-assisted UV photolysis with conventional photolithography and e-beam lithography techniques.

Direct laser writing technique has two major shortcomings, that is, low precision and substrate damage when used to pattern atomic-thick graphene films (see the Supporting Information, Figure S11).[12] In the etching process, a pulse laser with strong

https://dx.doi.org/10.1021/acsami.0c16005
ACS Appl. Mater. Interfaces 2020, 12, 55382−55389

peak intensity is a prerequisite to realize graphene patterning. If the UV discharge lamp is substituted by a vacuum UV laser, H_2O-based magnetic-assisted UV photolysis can convert into a chemically assisted direct laser writing approach with the following advantages. First, the vacuum UV laser can be a continuous one with much lower optical power since the photo-dissociated directional OH radicals play a major role in the etching efficiency. Second, the writing precision can be improved since the etching originates from a much shorter wavelength of a vacuum UV laser. Third, the adoption of a continuous low power laser can eliminate mechanical damage to the substrate underneath. We think chemically assisted direct laser writing can be an attractive topic in the future.

CONCLUSIONS

In summary, we have realized the patterning of a graphene film by the novel approach of H_2O-based magnetic-assisted UV photolysis. The photo-dissociated paramagnetic $H(1^2S)$ and $OH(X^2\Pi)$ radicals are magnetized in the inhomogeneous vertical magnetic field (B_z = 0.57 T, ∇B_z = 160 T·m^{-1}) and then turn into accelerated and directional motion toward graphene. Using the copper holey grids as the shadow mask, we can obtain graphene microstructures with the linewidth down to 8.5 μm. The H_2O-based magnetic-assisted UV photolysis has a capability of patterning 40 nm wide graphene nanoribbons under ZnO nanowires. The hybrid graphene/ZnO nanoribbon FET devices have the hole mobility up to 7200 cm^2·V^{-1}·s^{-1}. The functionality of $H(1^2S)$ and $OH(X^2\Pi)$ radicals in the graphene patterning has been ascertained. This work introduces a novel cost-effective approach of etching high-quality graphene micro-/nanoscale structures with high directionality, and it also opens up a new avenue of functionalizing and patterning the booming two-dimensional materials.[43−47]

METHODS

Strategy for Patterning Graphene Films by H_2O-Based Magnetic-Assisted UV Photolysis. Either high-quality single-crystal or polycrystalline CVD-grown monolayer graphene on copper foil was transferred onto the SiO_2 (300 nm)/Si (p^{++}) substrate taking the regularly used poly(methyl methacrylate)-mediated approach.[2,14] A home-designed UV vacuum machine equipped with a low-pressure mercury lamp[14] was used for graphene patterning. A 400-mesh copper grid (Gilder Grids AG400HS), a conventional sample support in tunneling electron microscopy, was put tightly on the graphene film as the shadow mask to pattern graphene microstructures. The chamber was first pumped to 2 × 10^{-3} Pa and then filled with gaseous H_2O molecules to 200 Pa (if not specified otherwise). In the H_2O-based magnetic-assisted UV photolysis, parameters including the working distance and UV irradiation were adjusted according to the specific micro/nano-structure of masks. Herein, a strategy of two to four cycles of UV exposure was taken to keep a high etching efficiency with the fixed initial H_2O pressure in the closed chamber, as well as to avoid excessive temperature rise in the UV photolysis. In order to carry out TOF-SIMS measurement, a graphite flake was treated for 120 s by D_2O-based magnetic-assisted UV photolysis with the initial gas pressure of 300 Pa.

Fabrication of Hybrid Graphene/ZnO Nanoribbon FET Devices. Graphene nanoribbon FET devices were fabricated utilizing ZnO nanowires, purchased from Nanjing XFNANO Materials Tech Co., Ltd., as the nanoscale shadow mask. The nanowires have a single crystal hexagon wurtzite structure with a diameter ranging from 50 to 120 nm and length from 5 to 50 μm. First, ZnO nanowires were dispersed into ethanol and stirred for 30 min before 8 min ultrasonic treatment at room temperature. Then, the solution was dripped onto graphene film and dried in the atmosphere to obtain individual ZnO nanowires (ready to use as masks). Next, Cr/Au (5 nm/90 nm) electrodes were thermally evaporated on ZnO nanowires using a copper shadow mask. Finally, we obtain hybrid graphene/ZnO nanoribbon FET devices by removing the exposed graphene by H_2O-based magnetic-assisted UV photolysis (working distance: 40 mm; duration: 9 min × 2 times). To obtain pure graphene nanoribbons, ZnO nanowires were etched off in a HCl/H_2O (1:20 volume ratio) chemical solution for 60 s.

Characterization. A gauss meter was used to measure the intensity and direction of the magnetic field near the graphene surface. The magnetic gradient was deduced from the magnetic variation upon a certain distance within 0.5 mm scope. A scanning electron microscope (Zeiss Ultra Plus) was used to obtain highly resolved topographic images under an accelerating voltage of 3 kV, if not specified elsewhere. Confocal micro-Raman spectroscopy (Renishaw inVia Qontor) was used to map graphene patterns by a laser at 532 nm (100× objective, ∼1.0 μm spot size) with the scanning step size of 1.0 μm. The electrical measurements were carried out in a nitrogen atmosphere at room temperature by a combination of Keithley 6430 and 2400 electrical systems. A Kratos Axis Ultra DLD spectrometer (equipped with a monochromatic Al Kα X-ray source) was used to obtain XPS spectra with the anode power of 150 W. A time-of-flight secondary ion mass spectrometer system (IONTOF 5-100) equipped with a Bi^+ beam source was used to acquire the chemical information of pristine graphite and that treated by H_2O-based magnetic-assisted UV photolysis under a bias of 30 keV. The scanning area was 100 μm × 100 μm with an acquisition time of 200 s. The software used for peak analysis was SurfaceLab 7.0. In order to reduce the influence from the atmospheric carbon, the samples freshly cleaved and those further treated by UV photolysis, were stored *in situ* in the low vacuum chamber (∼5 Pa) before being transferred into the corresponding high-vacuum chamber for XPS and TOF-SIMS measurements.

ASSOCIATED CONTENT

Supporting Information

The Supporting Information is available free of charge at https://pubs.acs.org/doi/10.1021/acsami.0c16005.

Influence of the shadow mask on graphene patterning, electrical transport property of a single ZnO nanowire, stabilization of ZnO nanowires treated by H_2O-based magnetic-assisted UV photolysis, patterning graphene film by D_2O-based magnetic-assisted UV photolysis, influence of an inhomogeneous vertical magnetic field on graphene patterning, patterning graphene film by oxygen plasma, patterning graphene film under a xenon excimer lamp, and patterning graphene film by direct laser writing technique (PDF)

AUTHOR INFORMATION

Corresponding Author

Haihua Tao − *State Key Laboratory of Advanced Optical Communication Systems and Networks, School of Physics and Astronomy, Shanghai Jiao Tong University, Shanghai 200240, China*; orcid.org/0000-0002-1111-8181; Email: tao.haihua@sjtu.edu.cn

Authors

Shubin Su − *State Key Laboratory of Advanced Optical Communication Systems and Networks, School of Physics and Astronomy, Shanghai Jiao Tong University, Shanghai 200240, China*

Hao Li − *State Key Laboratory of Advanced Optical Communication Systems and Networks, School of Physics and Astronomy, Shanghai Jiao Tong University, Shanghai 200240, China*

Jingxian Huang − *State Key Laboratory of Advanced Optical Communication Systems and Networks, School of Physics and*

Astronomy, Shanghai Jiao Tong University, Shanghai 200240, China

Zhibin Zhang − *State Key Laboratory for Mesoscopic Physics, Collaborative Innovation Center of Quantum Matter, School of Physics, Peking University, Beijing 100871, China*

Chenhui Liang − *State Key Laboratory of Advanced Optical Communication Systems and Networks, School of Physics and Astronomy, Shanghai Jiao Tong University, Shanghai 200240, China*

Wenxiang Jiang − *Key Laboratory of Artificial Structures and Quantum Control (Ministry of Education), Shenyang National Laboratory for Materials Science, School of Physics and Astronomy, Shanghai Jiao Tong University, Shanghai 200240, China*

Aolin Deng − *Key Laboratory of Artificial Structures and Quantum Control (Ministry of Education), Shenyang National Laboratory for Materials Science, School of Physics and Astronomy, Shanghai Jiao Tong University, Shanghai 200240, China*

Kaihui Liu − *State Key Laboratory for Mesoscopic Physics, Collaborative Innovation Center of Quantum Matter, School of Physics, Peking University, Beijing 100871, China;* orcid.org/0000-0002-8781-2495

Zhiwen Shi − *Key Laboratory of Artificial Structures and Quantum Control (Ministry of Education), Shenyang National Laboratory for Materials Science, School of Physics and Astronomy, Shanghai Jiao Tong University, Shanghai 200240, China; Collaborative Innovation Center of Advanced Microstructures, Nanjing 210093, China;* orcid.org/0000-0002-3928-2960

Dong Qian − *Key Laboratory of Artificial Structures and Quantum Control (Ministry of Education), Shenyang National Laboratory for Materials Science, School of Physics and Astronomy and Tsung-Dao Lee Institute, Shanghai Jiao Tong University, Shanghai 200240, China; Collaborative Innovation Center of Advanced Microstructures, Nanjing 210093, China*

Complete contact information is available at: https://pubs.acs.org/10.1021/acsami.0c16005

Notes

The authors declare the following competing financial interest(s): Shanghai Jiaotong University, along with the authors, has filed provisional patents on the technology and intellectual property reported here (patent application numbers CN 201810981805.7; title: Patterning graphene film by magnetic-assisted photochemical oxidation with a specific setup).

■ ACKNOWLEDGMENTS

This work was supported by National Natural Science Foundation of China (grant nos. 11204173, 11874261) and Natural Science Foundation of Shanghai (grant no. 18ZR1419100). We thank Prof. W. Gu and Prof. J. Chen from Shanghai Jiao Tong University (SJTU) for fruitful discussion. We thank Prof. X. Xie from Shanghai Institute of Microsystem and Information Technology (CAS), Prof. Y. Zhang from Fudan University, Prof. Z. Ni from Southeast University, and Prof. X. Chen, Prof. Z. Sheng, Prof. Y. Dan, and Prof. X. Jin from SJTU for their support. We thank Prof. S. Wang from Beijing Institute of Technology for her technical support. We thank Dr. Y. Qu from the Sixth Element (Changzhou) Materials Technology Co. Ltd. for providing polycrystalline graphene film. We thank L. He and R. Wang from Instrumental Analysis Center of SJTU and Y. Wang and M. Liu from Advanced Electronic Materials and Devices of SJTU for their technical support.

■ REFERENCES

(1) Li, X.; Cai, W.; An, J.; Kim, S.; Nah, J.; Yang, D.; Piner, R.; Velamakanni, A.; Jung, I.; Tutuc, E.; Banerjee, S. K.; Colombo, L.; Ruoff, R. S. Large-Area Synthesis of High-Quality and Uniform Graphene Films on Copper Foils. *Science* **2009**, *324*, 1312−1314.

(2) Xu, X.; Zhang, Z.; Qiu, L.; Zhuang, J.; Zhang, L.; Wang, H.; Liao, C.; Song, H.; Qiao, R.; Gao, P.; Hu, Z.; Liao, L.; Liao, Z.; Yu, D.; Wang, E.; Ding, F.; Peng, H.; Liu, K. Ultrafast Growth of Single-Crystal Graphene Assisted by a Continuous Oxygen Supply. *Nat. Nanotechnol.* **2016**, *11*, 930−935.

(3) Lin, L.; Zhang, J.; Su, H.; Li, J.; Sun, L.; Wang, Z.; Xu, F.; Liu, C.; Lopatin, S.; Zhu, Y.; Jia, K.; Chen, S.; Rui, D.; Sun, J.; Xue, R.; Gao, P.; Kang, N.; Han, Y.; Xu, H. Q.; Cao, Y.; Novoselov, K. S.; Tian, Z.; Ren, B.; Peng, H.; Liu, Z. Towards Super-Clean Graphene. *Nat. Commun.* **2019**, *10*, 1912.

(4) Huang, M.; Bakharev, P. V.; Wang, Z.-J.; Biswal, M.; Yang, Z.; Jin, S.; Wang, B.; Park, H. J.; Li, Y.; Qu, D.; Kwon, Y.; Chen, X.; Lee, S. H.; Willinger, M.-G.; Yoo, W. J.; Lee, Z.; Ruoff, R. S. Large-Area Single-Crystal AB-Bilayer and ABA-Trilayer Graphene Grown on a Cu/Ni(111) Foil. *Nat. Nanotechnol.* **2020**, *15*, 289−295.

(5) Bae, S.; Kim, H.; Lee, Y.; Xu, X.; Park, J.-S.; Zheng, Y.; Balakrishnan, J.; Lei, T.; Kim, H. R.; Song, Y., II; Kim, Y.-J.; Kim, K. S.; Özyilmaz, B.; Ahn, J.-H.; Hong, B. H.; Iijima, S. Roll-To-Roll Production of 30-Inch Graphene Films for Transparent Electrodes. *Nat. Nanotechnol.* **2010**, *5*, 574−578.

(6) Novoselov, K. S.; Geim, A. K.; Morozov, S. V.; Jiang, D.; Zhang, Y.; Dubonos, S. V.; Grigorieva, I. V.; Firsov, A. A. Electric Field Effect in Atomically Thin Carbon Films. *Science* **2004**, *306*, 666−669.

(7) Ho, D. H.; Sun, Q.; Kim, S. Y.; Han, J. T.; Kim, D. H.; Cho, J. H. Stretchable and Multimodal All Graphene Electronic Skin. *Adv. Mater.* **2016**, *28*, 2601−2608.

(8) Yong, K.; Ashraf, A.; Kang, P.; Nam, S. Rapid Stencil Mask Fabrication Enabled One-Step Polymer-Free Graphene Patterning and Direct Transfer for Flexible Graphene Devices. *Sci. Rep.* **2016**, *6*, 24890.

(9) Kalita, G.; Qi, L.; Namba, Y.; Wakita, K.; Umeno, M. Femtosecond Laser Induced Micropatterning of Graphene Film. *Mater. Lett.* **2011**, *65*, 1569−1572.

(10) Jessen, B. S.; Gammelgaard, L.; Thomsen, M. R.; Mackenzie, D. M. A.; Thomsen, J. D.; Caridad, J. M.; Duegaard, E.; Watanabe, K.; Taniguchi, T.; Booth, T. J.; Pedersen, T. G.; Jauho, A.-P.; Bøggild, P. Lithographic Band Structure Engineering of Graphene. *Nat. Nanotechnol.* **2019**, *14*, 340−346.

(11) Zhang, L.; Diao, S.; Nie, Y.; Yan, K.; Liu, N.; Dai, B.; Xie, Q.; Reina, A.; Kong, J.; Liu, Z. Photocatalytic Patterning and Modification of Graphene. *J. Am. Chem. Soc.* **2011**, *133*, 2706−2713.

(12) Bell, D. C.; Lemme, M. C.; Stern, L. A.; Williams, J. R.; Marcus, C. M. Precision Cutting and Patterning of Graphene with Helium Ions. *Nanotechnology* **2009**, *20*, 455301.

(13) Kolmer, M.; Steiner, A.-K.; Izydorczyk, I.; Ko, W.; Engelund, M.; Szymonski, M.; Li, A.-P.; Amsharov, K. Rational Synthesis of Atomically Precise Graphene Nanoribbons Directly on Metal Oxide Surfaces. *Science* **2020**, *369*, 571−575.

(14) Wu, Y.; Tao, H.; Su, S.; Yue, H.; Li, H.; Zhang, Z.; Ni, Z.; Chen, X. Patterning Graphene Film by Magnetic-Assisted UV Ozonation. *Sci. Rep.* **2017**, *7*, 46583.

(15) Yue, H.; Tao, H.; Wu, Y.; Su, S.; Li, H.; Ni, Z.; Chen, X. Exploring the Working Mechanism of Graphene Patterning by Magnetic-Assisted UV Ozonation. *Phys. Chem. Chem. Phys.* **2017**, *19*, 27353−27359.

(16) He, T.; Wang, Z.; Zhong, F.; Fang, H.; Wang, P.; Hu, W. Etching Techniques in 2D Materials. *Adv. Mater. Technol.* **2019**, *4*, 1900064.

(17) Koizumi, K.; Boero, M.; Shigeta, Y.; Oshiyama, A. Atom-Scale Reaction Pathways and Free-Energy Landscapes in Oxygen Plasma Etching of Graphene. *J. Phys. Chem. Lett.* **2013**, *4*, 1592−1596.

(18) Nojiri, K. *Dry Etching Technology for Semiconductors*; Spring International Publishing: Switzerland, 2015.
(19) Fujishima, A.; Honda, K. Electrochemical Photolysis of Water at a Semiconductor Electrode. *Nature* **1972**, *238*, 37−38.
(20) Takata, T.; Jiang, J.; Sakata, Y.; Nakabayashi, M.; Shibata, N.; Nandal, V.; Seki, K.; Hisatomi, T.; Domen, K. Photocatalytic Water Splitting with a Quantum Efficiency of Almost Unity. *Nature* **2020**, *581*, 411−414.
(21) Plusquellic, D. F.; Votava, O.; Nesbitt, D. J. Photodissociation Dynamics of Jet-Cooled H_2O and D_2O in the Non-Franck−Condon Regime: Relative Absorption Cross Sections and Product State Distributions at 193 nm. *J. Chem. Phys.* **1997**, *107*, 6123−6135.
(22) Yang, X. F.; Hwang, D. W.; Lin, J. J.; Ying, X. Dissociation Dynamics of the Water Molecule on the $\tilde{A}^1B_1$ Electronic Surface. *J. Chem. Phys.* **2000**, *113*, 10597−10604.
(23) Wang, H.-t.; Felps, W. S.; McGlynn, S. P. Molecular Rydberg States. VII. Water. *J. Chem. Phys.* **1977**, *67*, 2614−2628.
(24) David, D.; Bar, I.; Rosenwaks, S. Doppler Polarization Spectroscopy of the Photofragments from an In-Plane Rotation of Water: Demonstration of Unperturbed Vector Correlations. *J. Phys. Chem.* **1993**, *97*, 11571−11574.
(25) Vincenzo, B.; Paola, C.; Alberto, J. *Photochemistry and Photophysics: Concepts, Research, Applications*; Wiley-VCH Verlag GmbH & Co. KGaA: Weinheim, Germany, 2014.
(26) Radich, J. G.; Kamat, P. V. Making Graphene Holey. Gold-Nanoparticle-Mediated Hydroxyl Radical Attach on Reduced Graphene Oxide. *ACS Nano* **2013**, *7*, 5546−5557.
(27) Haynes, W. M.; Lide, D. R.; Bruno, T. J. *CRC Handbook of Chemistry and Physics*, 97th ed.; CRC Press Taylor & Francis Group: Boca Raton, 2016−2017.
(28) Stuhl, B. K.; Hummon, M. T.; Yeo, M.; Quéméner, G.; Bohn, J. L.; Ye, J. Evaporative Cooling of the Dipolar Hydroxyl Radical. *Nature* **2012**, *492*, 396−400.
(29) Tinkham, M.; Strandberg, M. W. P. Interaction of Molecular Oxygen with a Magnetic Field. *Phys. Rev.* **1955**, *97*, 951−966.
(30) Taft, H.; Dailey, B. P. Magnetic Susceptibility of the H_2O Molecule. *J. Chem. Phys.* **1969**, *51*, 1002−1007.
(31) Phipps, T. E.; Taylor, J. B. The Magnetic Moment of Atomic Hydrogen. *Science* **1926**, *64*, 480−481.
(32) Blundell, S. *Magnetism in Condensed Matter*; Oxford University Press Inc.: New York, 2001.
(33) Šljivančanin, Ž.; Rauls, E.; Hornekær, L.; Xu, W.; Besenbacher, F.; Hammer, B. Extended Atomic Hydrogen Dimer Configurations on the Graphite (0001) Surface. *J. Chem. Phys.* **2009**, *131*, 084706.
(34) Balog, R.; Jørgensen, B.; Wells, J.; Lægsgaard, E.; Hofmann, P.; Besenbacher, F.; Hornekær, L. Atomic Hydrogen Adsorbate Structures on Graphene. *J. Am. Chem. Soc.* **2009**, *131*, 8744−8745.
(35) Elias, D. C.; Nair, R. R.; Mohiuddin, T. M. G.; Morozov, S. V.; Blake, P.; Halsall, M. P.; Ferrari, A. C.; Boukhvalov, D. W.; Katsnelson, M. I.; Geim, A. K.; Novoselov, K. S. Control of Graphene's Properties by Reversible Hydrogenation: Evidence for Graphane. *Science* **2009**, *323*, 610−613.
(36) Shi, Z.; Yang, R.; Zhang, L.; Wang, Y.; Liu, D.; Shi, D.; Wang, E.; Zhang, G. Patterning Graphene with Zigzag Edges by Self-Aligned Anisotropic Etching. *Adv. Mater.* **2011**, *23*, 3061−3065.
(37) Chou, H.; Ismach, A.; Ghosh, R.; Ruoff, R. S.; Dolocan, A. Revealing the Planar Chemistry of Two-Dimensional Heterostructures at the Atomic Level. *Nat. Commun.* **2015**, *6*, 7482.
(38) Wallace, J. S.; Quinn, A.; Gardella, J. A., Jr.; Hu, J.; Kong, E. S.-W.; Joh, H.-I. Time-Of-Flight Secondary Ion Mass Spectrometry as a Tool for Evaluating the Plasma-Induced Hydrogenation of Graphene. *J. Vac. Sci. Technol., B: Nanotechnol. Microelectron.: Mater., Process., Meas., Phenom.* **2016**, *34*, 03H113.
(39) Xie, W.; Weng, L.-T.; Ng, K. M.; Chan, C. K.; Chan, C.-M. Clean Graphene Surface through High Temperature Annealing. *Carbon* **2015**, *94*, 740−748.
(40) Engel, V.; Schinke, R.; Staemmler, V. Photodissociation Dynamics of H_2O and D_2O in the First Absorption Band: A Complete *ab initio* Treatment. *J. Chem. Phys.* **1988**, *88*, 129−148.
(41) Harich, S. A.; Yang, X.; Hwang, D. W. H.; Lin, J. J.; Yang, X.; Dixon, R. N. Photodissociation of D_2O at 121.6 nm: A State-To-State Dynamical Picture. *J. Chem. Phys.* **2001**, *114*, 7830−7837.
(42) Mulcahy, M. F. R.; Young, B. C. The Reaction of Hydroxyl Radicals with Carbon at 298 K. *Carbon* **1975**, *13*, 115−124.
(43) Lee, J. S.; Choi, S. H.; Yun, S. J.; Kim, Y. I.; Boandoh, S.; Park, J.-H.; Shin, B. G.; Ko, H.; Lee, S. H.; Kim, Y.-M.; Lee, Y. H.; Kim, K. K.; Kim, S. M. Wafer-Scale Single-Crystal Hexagonal Boron Nitride Film *via* Self-Collimated Grain Formation. *Science* **2018**, *362*, 817−821.
(44) Wang, L.; Xu, X.; Zhang, L.; Qiao, R.; Wu, M.; Wang, Z.; Zhang, S.; Liang, J.; Zhang, Z.; Zhang, Z.; Chen, W.; Xie, X.; Zong, J.; Shan, Y.; Guo, Y.; Willinger, M.; Wu, H.; Li, Q.; Wang, W.; Gao, P.; Wu, S.; Zhang, Y.; Jiang, Y.; Yu, D.; Wang, E.; Bai, X.; Wang, Z.-J.; Ding, F.; Liu, K. Epitaxial Growth of a 100-Square-Centimetre Single-Crystal Hexagonal Boron Nitride Monolayer on Copper. *Nature* **2019**, *570*, 91−95.
(45) Chen, T.-A.; Chuu, C.-P.; Tseng, C.-C.; Wen, C.-K.; Wong, H.-S. P.; Pan, S.; Li, R.; Chao, T.-A.; Chueh, W.-C.; Zhang, Y.; Fu, Q.; Yakobson, B. I.; Chang, W.-H.; Li, L.-J. Wafer-Scale Single-Crystal Hexagonal Boron Nitride Monolayers on Cu (111). *Nature* **2020**, *579*, 219−223.
(46) Andrzejewski, D.; Myja, H.; Heuken, M.; Grundmann, A.; Kalisch, H.; Vescan, A.; Kümmell, T.; Bacher, G. Scalable Large-Area p-i-n Light-Emitting Diodes Based on WS_2 Monolayers Grown *via* MOCVD. *ACS Photonics* **2019**, *6*, 1832−1839.
(47) Park, Y. J.; Sharma, B. K.; Shinde, S. M.; Kim, M.-S.; Jang, B.; Kim, J.-H.; Ahn, J.-H. All MoS_2-Based Large Area, Skin-Attachable Active-Matrix Tactile Sensor. *ACS Nano* **2019**, *13*, 3023−3030.

https://dx.doi.org/10.1021/acsami.0c16005
ACS Appl. Mater. Interfaces 2020, 12, 55382−55389